

MULTIPATH PROPAGATION CHARACTERIZATION FOR TERRESTRIAL MOBILE AND FIXED MICROWAVE COMMUNICATIONS

Thesis for the degree of Doctor of Science in Technology

Xiongwen Zhao



TEKNILLINEN KORKEAKOULU
TEKNISKA HÖGSKOLAN
HELSINKI UNIVERSITY OF TECHNOLOGY
TECHNISCHE UNIVERSITÄT HELSINKI
UNIVERSITE DE TECHNOLOGIE D'HELSINKI

Helsinki University of Technology Radio Laboratory Publications

Teknillisen korkeakoulun Radiolaboratorion julkaisuja

Espoo, October, 2002

REPORT S 256

MULTIPATH PROPAGATION CHARACTERIZATION FOR TERRESTRIAL MOBILE AND FIXED MICROWAVE COMMUNICATIONS

Xiongwen Zhao

Dissertation for the degree of Doctor of Science in Technology to be presented with due permission for public examination and debate in Auditorium S4 at Helsinki University of Technology (Espoo, Finland) on the 13th of December 2002 at 12 o'clock noon.

Helsinki University of Technology

Department of Electrical and Communications Engineering

Radio Laboratory

Teknillinen korkeakoulu

Sähkö- ja tietoliikennetekniikan osasto

Radiolaboratorio

Distribution:

Helsinki University of Technology

Radio Laboratory

P.O.Box 3000

FIN-02015 HUT

Tel. +358-9-451 2252

Fax. +358-9-451 2152

© Xiongwen Zhao and Helsinki University of Technology Radio Laboratory

ISBN 951-22- 6164-2

ISSN 1456-3835

Otamedia Oy

Espoo 2002

PREFACE

This thesis has been carried out at the Radio Laboratory of Institute of Digital Communications in Helsinki University of Technology during October 1998 – May 2002. During this period, I mainly worked for LALAMO (Wireless Wideband Modems) project funded by TEKES, coordinated by VTT Electronics and supported by Elektrobit Oyj, Nokia Networks and Elisa Communications. Some parts of the work had been done when I worked in China Research Institute of Radiowave Propagation (CRIRP). I thank the LALAMO project for funding my research work, which made this thesis possible.

First and foremost I would like to thank my supervisor, Prof. Pertti Vainikainen, for his very helpful guidance, the numerous novel ideas and encouragement during all my work. I would like to thank Prof. Antti Räisänen very much for his encouragement and support. I thank Dr. Jarmo Kivinen for fruitful discussions in many aspects and very good cooperation in the project work, Dr. Ioannis T. Rekanos for helpful discussions, and Stina Lindberg for her excellent work and kindness.

I thank my thesis pre-examiners Prof. Andreas F. Molisch and Dr. Wei Zhang for their helpful comments and suggestions.

Last but not least I would like to thank my wife Suiyan Geng and my daughter Gengjing Zhao for their love, patience and understanding, and my parents for their endless encouragement.

Helsinki, October, 2002.

Xiongwen Zhao

ABSTRACT

Multipath propagation is a key issue studied throughout this thesis, and it causes dispersions in delay, frequency and spatial domains. These are dominant phenomena in both terrestrial mobile and fixed wideband communications. In this thesis, multipath propagation mechanisms including diffraction, refraction, reflection and scattering are studied when radio waves interact with dielectric and metallic objects, or an atmospheric duct. Measurements were also performed for empirical modelling and validation of the theoretical work carried out in this thesis.

By using physical optics (PO) method, the attenuation by double knife edges with ground reflections is solved for the first time under a general formula of the attenuation by multiple knife edges with ground reflections derived in this thesis, and some important and interesting conclusions are obtained. The attenuations by curvilinear-topped obstacles and by multiple flat-topped obstacles are also presented in closed forms. The results are the simplest and easiest ones available now, and they can be applied for field strength predictions both in mobile and fixed microwave communications.

Based on three-ray (direct, reflected and super-refracted) and two-ray (direct and super-refracted) multipath models for plane and spherical earth, respectively, frequency selective fading (FSF) and depolarization due to clear air are studied by simulations and experiments for terrestrial line-of-sight (LOS) microwave links and dual-polarized communication systems. Novel simulation methods have been introduced and applied based on the fact that the amplitudes and excess delays of the rays are functions of the (modified) refractive index gradients which are random variables with exponential and normal distributions inside and outside the duct in lower atmosphere, respectively.

Some important empirical or semi-empirical models and parameters are presented at 5 GHz based on large amount of measured data in indoor and outdoor environments. The results include path loss models, excess delay and rms delay spread, spatial and frequency correlations, window (sector) length of averaging fast fading components, path number distribution, and tapped-delay-line (TDL) channel models. These empirical or semi-empirical parameters and models are the latest results achieved at 5 GHz, and they are of great importance in designing of future wireless local area networks (WLAN), especially the TDL models are developed for the first time in this frequency band.

Using a general autocorrelation function derived in this thesis for three-dimensional (3-D) scattering environments, a novel theoretical modelling method is developed to study the propagation mechanisms of different types of Doppler spectra observed in measurements. The 3-D autocorrelation function is connected to the probability density functions (PDF) of the angles of arrival (AoAs) of the scattered waves and the antenna radiation patterns in the azimuth and elevation planes. This is a new work which tries to define and explain the physical reasons of 3-D Doppler spectra from propagation point of view.

A new computer simulation method for wideband 3-D received signal level in an urban environment is developed under the general assumptions of the distributions for path number, amplitude, excess delay etc. This simulation method can provide detailed fading characteristics for wideband mobile communications in a specific urban environment.

CONTENTS

PREFACE	3
ABSTRACT..	4
CONTENTS	5
LIST OF PUBLICATIONS	7
1. INTRODUCTION	9
2. DIFFRACTION OVER TERRAIN OBSTACLES	11
2.1 INTRODUCTION	11
2.2 UTD METHOD FOR A PERFECTLY CONDUCTING WEDGE.....	11
2.3 PHYSICAL OPTICS (PO) APPLIED TO A FLAT-TOPPED TERRAIN OBSTACLE	12
2.4 THE NEW APPLICATIONS OF PO FOR TERRAIN FIELD STRENGTH PREDICTIONS.....	13
2.4.1 <i>Attenuation by multiple knife edges with ground reflections.....</i>	<i>13</i>
2.4.2 <i>Attenuation by curvilinear-topped obstacles and multiple flat-topped obstacles.....</i>	<i>14</i>
3. MULTIPATH PROPAGATION STUDIES FOR TERRESTRIAL MICROWAVE COMMUNICATIONS	16
3.1 INTRODUCTION	16
3.2 THE ATMOSPHERIC DUCT AND THE METEOROLOGICAL CONDITION	16
3.3 THE CUMULATIVE DISTRIBUTIONS FOR REFRACTIVE INDEX GRADIENTS IN LOWER ATMOSPHERE	17
3.4 EXPERIMENTAL AND COMPUTER SIMULATION STUDIES OF FREQUENCY SELECTIVE FADING	17
3.4.1 <i>Transfer function of multipath channel.....</i>	<i>17</i>
3.4.2 <i>Computer simulation method</i>	<i>18</i>
3.4.3 <i>Measurement setup</i>	<i>20</i>
3.5 COMPUTER SIMULATION STUDIES OF DEPOLARIZATION DUE TO CLEAR AIR	21
4. PROPAGATION CHARACTERIZATION OF RADIO CHANNELS FOR FUTURE WLAN MOBILE COMMUNICATION SYSTEMS	23
4.1 INTRODUCTION	23
4.2 BASIC PROPAGATION CONCEPTS AND MODELLING PARAMETERS	23
4.3 TAPPED DELAY LINE CHANNEL MODELS	27
4.4 PROPAGATION MECHANISM STUDIES FOR DIFFERENT TYPES OF DOPPLER SPECTRA	28
4.4.1 <i>Formulation of theoretical Doppler spectrum modelling.....</i>	<i>28</i>
4.4.2 <i>Empirical Doppler spectrum model.....</i>	<i>29</i>
4.5 A GENERAL COMPUTER SIMULATION METHOD FOR 3-D RECEIVED SIGNAL LEVEL IN WIDEBAND MOBILE COMMUNICATIONS	29

5. SUMMARY OF PUBLICATIONS	31
6. CONCLUSION	33
ERRATA	34
REFERENCES	35
PUBLICATIONS [P1] – [P8]	

LIST OF PUBLICATIONS

This thesis is based on the following journal papers:

- [P1] **X. Zhao** and P. Vainikainen, "Multipath Propagation Study Combining Terrain Diffraction and Reflection," *IEEE Transactions on Antennas and Propagation*, vol. 49, no. 8, pp. 1204-1209, Aug. 2001.
- [P2] **X. Zhao**, P. Vainikainen, and J. Kivinen, "Diffraction over Typical-Shaped Terrain Obstacles," *Journal of Electromagnetic Waves and Applications*, vol. 13, no. 12, pp. 1691-1707, Dec. 1999.
- [P3] **X. Zhao**, Y. Zhang, P. Vainikainen, and Y. Xie, "The Experimental and Computer Simulation Studies of Frequency Selective Fading in Line-of-Sight Terrestrial Microwave Links," *Radio Science*, vol. 36, no. 6, pp. 1393-1403, Nov.-Dec. 2001.
- [P4] **X. Zhao** and P. Vainikainen, "Computer Simulation of Multipath Depolarization due to Clear Air," *Microwave and Optical Technology Letters*, vol. 23, no. 1, pp. 4-7, Oct. 1999.
- [P5] **X. Zhao**, J. Kivinen, P. Vainikainen, and K. Skog, "Propagation Characteristics for Wideband Outdoor Mobile Communications at 5.3 GHz," *IEEE Journal on Selected Areas in Communications*, vol. 20, no. 3, pp. 507-514, Apr. 2002.
- [P6] J. Kivinen, **X. Zhao**, and P. Vainikainen, "Empirical Characterization of Wideband Indoor Radio Channel at 5.3 GHz," *IEEE Transactions on Antennas and Propagation*, vol. 49, no. 8, pp. 1192-1203, Aug. 2001.
- [P7] **X. Zhao**, J. Kivinen, P. Vainikainen, and K. Skog, "Characterization of Doppler Spectra for Mobile Communications at 5.3 GHz," accepted for publication in *IEEE Transactions on Vehicular Technology*, May, 2002.
- [P8] **X. Zhao**, I. T. Rekanos, and P. Vainikainen, "A General Computer Simulation Method for 3-D Received Signal Level in Wideband Mobile Communications," *Microwave and Optical Technology Letters*, vol. 32, no. 2, pp. 119-122, Jan. 2002.

In [P1][P2], this author derived all the theoretical results, completed the numerical calculations and prepared the manuscript. The work was supervised by Pertti Vainikainen. [P3] is a joint work, this author had the main responsibility in preparing the paper, processing the measured data and developing the experimental and computer simulation models in the paper. The experimental system was developed by research group 902 in CRIRP. The computer simulation frame and codes were mainly developed by Yerong Zhang. This author's work was supervised by Pertti Vainikainen. In [P4], this author developed the computer simulation method and prepared the manuscript. This author's work was supervised by Pertti Vainikainen. In [P5] and [P7], this author had the main responsibility of both theoretical and experimental modelling work and preparing the manuscripts. Jarmo Kivinen upgraded the measurement system suitable for the measurement campaigns, performed data preprocessing and made some contributions in the modeling work for the rotation measurement. Kari Skog planned and

organized the measurement campaigns. In [P6], this author mainly developed the tapped-delay-line channel models and participated in the measurement campaign. In [P5]-[P7], this author was supervised by Pertti Vainikainen and Jarmo Kivinen. In [P8], this author had the main responsibility of both the theoretical and simulation work and prepared the manuscript. Ioannis T. Rekanos wrote the code for generating Poisson random numbers and this author's work was supervised by Pertti Vainikainen.

1. INTRODUCTION

Multipath propagation is a key issue faced in all wideband mobile and fixed communications, and it causes delay dispersion and frequency selective fading in delay and frequency domains, respectively. They are the main reasons to cause performance degradation for wideband communication systems. The mechanisms which govern radio propagation are complex and diverse, and they can generally be attributed by reflection, diffraction, refraction and scattering or their combinations according to a specific environment and the frequency band. The frequencies covered in this thesis are mainly at microwave bands. For mobile communications, the frequency band is focused on 5.3 GHz for future wireless local area network (WLAN) mobile systems. Frequency selective fading (FSF) and depolarization due to multipath propagation caused by anomalous atmospheric conditions are studied at 2.2 and 7.6 GHz, respectively, for medium or large capacity line-of-sight (LOS) terrestrial microwave links and dual-polarized communication systems.

The propagation mechanisms covered in this thesis include diffraction, refraction, reflection and scattering. Diffraction occurs when the radio path between the transmitter and receiver is obstructed by an impenetrable body. Based on Huygens' principle, secondary waves are formed behind the obstructing body. The diffraction study in this work is mainly based on physical optics (PO). The attenuation by double knife edges with ground reflections is solved for the first time using a general formula derived in this thesis for the attenuation by multiple knife edges with ground reflections. The attenuations by curvilinear-topped obstacles and multiple flat-topped obstacles are also solved by calculating the field components which are related to Vogler's multiple knife-edge field of attenuation [1].

Refraction study discussed in this thesis is for terrestrial microwave communication links. A super-refractive ray occurs when an atmospheric duct has been formed. The multipath models considered here are three-ray (direct, reflected and super-refracted) and two-ray (direct and super-refracted) models in frequency selective fading and depolarization studies for terrestrial microwave links and dual polarized communication systems, respectively. In this thesis, novel simulation methods are introduced for the studies in these areas. Refraction phenomenon can be neglected for micro- and pico-cellular mobile communications due to the short distance between base and mobile stations. However, in macro-cellular systems, if the distance between base and mobile station is large, for example, several tens of kilometres, the effect of the troposphere should be taken into account.

Reflection occurs when a propagating electromagnetic wave impinges upon an obstruction with dimensions very large compared to the wavelength. Reflection rays from different surfaces may interfere constructively or destructively at a receiver. Scattering occurs when the radio channel contains objects with dimensions that are on the order of or smaller than the propagating wavelength. Scattering, which follows the same physical principles as diffraction, causes energy to be radiated in many different directions. Scattering [2] has been proven to be the most difficult of the three propagation mechanisms and it also makes the theoretical prediction more complicated. However, scattering can be neglected in many cases compared to the field contributions by diffraction, reflection, combination of reflection(s) and diffraction(s), and/or transmission.

Multipath propagation mechanisms for mobile communications are more complicated than for terrestrial microwave links, which makes theoretical studies and simulations more difficult and sometimes unpractical and unreliable. Therefore, measurements are also important to

characterize the radio channels. In this thesis, the radio channel sounder at 5.3 GHz developed at the Institute of Digital Communications (IDC) of Helsinki University of Technology (HUT) [3][4] has been used in the measurement campaigns. Some important empirical or semi-empirical models and parameters are developed/derived at 5.3 GHz, such as path loss models, excess delay and rms delay spread, spatial and frequency correlations, window (sector) length of averaging fast fading components, path number distribution, and tapped-delay-line (TDL) channel models. These empirical or semi-empirical parameters and models are the latest results achieved at 5.3 GHz, and they are of great importance for future WLAN mobile systems.

Another important aspect in this thesis is about the propagation mechanism studies for different types of Doppler spectra observed in measurements. This is new work which tries to define and explain the physical reasons for three-dimensional (3-D) Doppler spectra from propagation point of view. In this work, general methods are introduced about how to derive the Doppler spectra from theoretical simulations and measurements, where the radio channel should be assumed as wide sense stationary uncorrelated scattering (WSSUS) channel.

For urban multipath scattered environments, a new simulation method is introduced for wideband 3-D received signal level over a short mobile moving distance under some general assumptions of the distributions for path number, amplitude, excess delay etc. The simulation method can provide detailed fading characteristics in specific urban environments.

2. DIFFRACTION OVER TERRAIN OBSTACLES

2.1 INTRODUCTION

Uniform theory of diffraction (UTD) and physical optics (PO) or Fresnel-Kirchhoff (F-K) theory are the basic methods in solving terrain diffraction propagation problems. In the following the basic theories for the two methods are summarized and the main point will be focused on the PO and its applications.

UTD is a quite convenient method to calculate the diffraction field by a single wedge. However, due to the fact that the fields in the transition regions do not have optical behaviour, higher order diffraction fields should be considered for multiple wedges with overlapping transition regions [5]. Otherwise the fields are not continuous at the boundaries of the inside and outside of the transition regions.

In terrestrial microwave links and macro-cellular mobile communications, terrain obstacles have often been modelled as knife edges. The field is found as a function of height above each knife edge in turn. In each step, according to Huygens' principle the field above the next knife edge is found using the known field above the previous knife edge [1]. The analysis is then extended by bridging the spaces between the knife edges with planar reflecting surfaces and including the reflected wave field.

2.2 UTD METHOD FOR A PERFECTLY CONDUCTING WEDGE

Geometrical optics (GO) cannot predict the field in a shadow region caused for example, by a wedge. In the vicinity of the shadow boundary the results of the GO are also inaccurate [6]. The shortcoming of the GO, when it is used to predict fields in shadow regions, was overcome by Keller [7], who formulated the geometrical theory of diffraction (GTD). However, the GTD does not remove the inaccuracy in the vicinity of the shadow boundaries. The difficulties in the transition regions near the incidence and reflection boundaries were removed by UTD [8] and the diffraction coefficient for a conducting wedge can be expressed as follows

$$D_s = D_s(L, n; \phi, \phi'; \beta_0) = D^{(1)} + D^{(2)} - [D^{(3)} + D^{(4)}] \quad (1)$$

$$D_h = D_h(L, n; \phi, \phi'; \beta_0) = D^{(1)} + D^{(2)} + [D^{(3)} + D^{(4)}] \quad (2)$$

where D_s and D_h are the diffraction coefficients for soft (horizontal polarization) and hard (vertical polarization) boundary conditions. The components $D^{(l)}$ ($l = 1, 2, 3, 4$) of the diffraction in (1) and (2) are given by

$$D^{(l)} = D^{(l)}(L, n; \phi, \phi'; \beta_0) = \frac{-e^{-i\pi/4}}{2n\sqrt{2\pi k \sin \beta_0}} \cot \gamma^{(l)} F_0(2kLn^2 \sin^2 \gamma^{(l)}) \quad (3)$$

where k is wave number, i is the imaginary unit, $(2-n)\pi$ is the interior angle of the wedge, and ϕ' and ϕ are incidence and diffraction angles shown in Fig. 1 for 0-face and n -face,

respectively. L is called the distance parameter, which is related to the type of the incident wave. For example, if the incident wave is spherical, then $L = \frac{ss'}{s+s'} \sin^2 \beta_0$, where β_0 is the angle between the incident ray and the edge of the wedge. The transition function F_0 is defined as follows

$$F_0(x) = 2i\sqrt{x} \exp(ix) \int_{\sqrt{x}}^{\infty} \frac{\exp(-it^2)}{t} dt \quad (4)$$

The $\gamma^{(l)}$ in (3) can be found in [9]. In [9], the recent research results put forward in [10][11] have been applied, which removes the integer N^\pm defined in [8]. However, (3) does not give significantly different results. Instead, it provides some computational simplification.

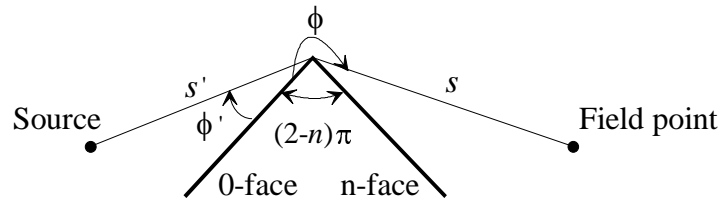


Fig. 1 Ray geometry for diffraction by a wedge

The result by using the diffraction coefficients shown in (1) and (2) is valid everywhere in space as long as the fields are ray optical. The UTD is a ray-based theory, thus, difficulties arise when the incident field is not ray optical. This can occur in the case of double diffraction problems. Here, we can have diffraction of a transition region field due either to the incident or to the reflection boundary which do not have a ray optical behaviour [12][13]. This insufficiency is even more pronounced for overlapping transition regions, when we deal with shadow boundaries, where the source, the wedges and the field points are (or nearly are) on a straight line [14]. In this case, the coupling of the two wedges is serious. In other words, the diffraction events can not be regarded as local phenomena. However, in a region outside the overlapping transition regions, which is in a region involving one transition region at most, conventional UTD augmented by slope diffraction [6], [15]-[17] can yield a good result. A detailed discussion about slope diffraction and the field in the transition regions for multipath knife edges are available in [18]. If an inclusion of the second-order field does not give accurate enough results, higher order diffraction fields are needed [5]. Moreover, such fields can be used for diffraction by three or more wedges.

2.3 PHYSICAL OPTICS (PO) APPLIED TO A FLAT-TOPPED TERRAIN OBSTACLE

A two-dimensional flat-topped obstacle is shown in Fig. 2, where $j, j+1$ are the two adjacent knife edges which extend to infinity along the y -axis, x_j and x_{j+1} are the positions of knife edges, k is the wave number, R_F is the reflection coefficient of the flat top, and ξ_j and ξ_{j+1} are the heights of the two knife edges relative to the height of the transmitter. Based on Helmholtz integral and considering small wave, paraxial approximation, the field relative to free space at the receiving point is expressed as [19]

$$\hat{E}(x_{j+1}, z_{j+1}) = \left(\frac{kx_{j+1}}{2\pi i x_j \Delta x_j} \right)^{\frac{1}{2}} \left[\int_{\xi_j}^{\infty} \hat{E}(x_j, z_j) e^{ikr} dz_j + \int_{\xi_j}^{\infty} \hat{E}(x_j, z_j) \cdot R_F e^{ikr'} dz_j \right] \quad (5)$$

where

$$r = \frac{x_{j+1}}{2x_j \Delta x_j} \left(z_j - \frac{x_j}{x_{j+1}} z_{j+1} \right)^2 \quad (6)$$

where $\Delta x_j = x_{j+1} - x_j$, $r' = r + 2h_1 h_2 / \Delta x_j$ and $h_1 = z_j - \xi_j$, $h_2 = z_{j+1} - \xi_{j+1}$.

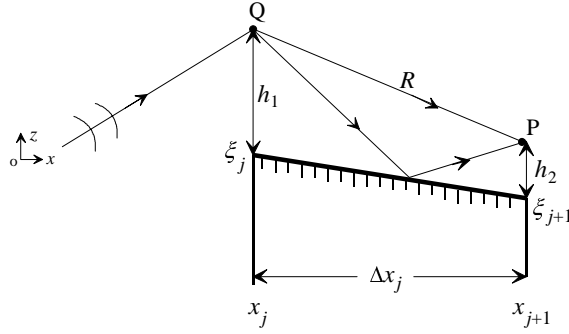


Fig. 2 The problem of finding the field at P due to a Huygens' point source at Q

2.4 THE NEW APPLICATIONS OF PO FOR TERRAIN FIELD STRENGTH PREDICTION

Based on the work of [19][20], attenuation by double knife edges with ground reflections, attenuations by curvilinear-topped obstacles and multiple flat-topped obstacles are solved in [P1] and [P2], respectively.

2.4.1 Attenuation by multiple knife edges with ground reflections

As shown in Fig. 3, assume that there are N knife edges and that at the interval (x_j, x_{j+1}) the reflection coefficient is R_{Fj+1} . The time dependence is given by $e^{-i\omega t}$, where i is the imaginary unit. From (5) and with some mathematical transformations, the field relative to free space at point R can be derived as

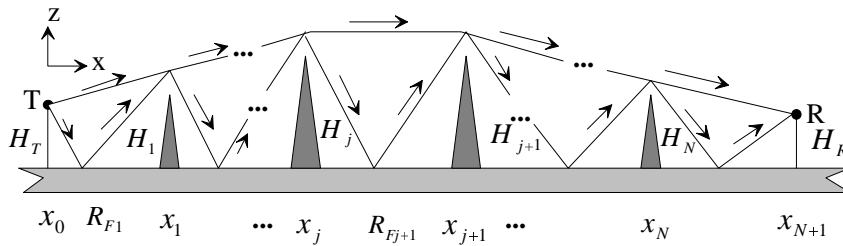


Fig. 3 Geometry for calculating knife-edge diffraction with ground reflections

$$\hat{E}(x_{N+1}, z_{N+1}) = \left(\frac{k}{2\pi i} \right)^{\frac{N}{2}} \left(\frac{x_{N+1}}{x_1 \Delta x_1 \cdots \Delta x_N} \right)^{\frac{1}{2}} \int_{H_1, H_2}^{\infty} \int_{H_2}^{\infty} \cdots \int_{H_N}^{\infty} dz_1 dz_2 \cdots dz_N$$

$$\left[1 + R_{F1} \exp \left(ik \frac{2z_1 H_T}{x_1} \right) \right] \prod_{j=1}^N \left[\exp(ikr_j) + R_{Fj+1} \exp(ikr_j') \right] \quad (7)$$

where

$$r_j = \frac{x_{j+1}}{2x_j \Delta x_j} \left[z_j - H_T - \frac{x_j}{x_{j+1}} (z_{j+1} - H_T) \right]^2 \quad (8)$$

$$r_j' = \frac{x_{j+1}}{2x_j \Delta x_j} \left[z_j - H_T + \frac{x_j}{x_{j+1}} (z_{j+1} - H_T) \right]^2 + \frac{2(z_j + z_{j+1})H_T}{\Delta x_j} - \frac{2H_T^2}{\Delta x_j} \quad (9)$$

where H_T , H_R and H_1, H_2, \dots, H_N are the heights relative to ground for the transmitter, receiver and multiple knife edges, respectively. In [P1], the attenuation of double knife edges with ground reflections is solved. The final received field is the sum of eight field components and each contains the Fresnel surface integral

$$\left(-\frac{i}{2} \right) \int_q^{\infty} \int_{u_0 \pm mv+n}^{\infty} \exp \left[i \frac{\pi}{2} (u^2 + v^2) \right] dudv \quad (10)$$

where q , u_0 , m and n are constants. Based on numerical calculations in [P1], the multipath field components can be reduced by locating where is the main reflection point. The surface reflection (if exists) cannot be neglected between the last knife edge and the receiver where it is in the diffraction region. The solutions of (10) can be found [14][20][21].

2.4.2 Attenuation by curvilinear-topped obstacles and multiple flat-topped obstacles

For a curvilinear-topped obstacle, the relative field of attenuation was also solved in [22], but a complicated series was included in the final results. In [P2], a quite simple and symmetrical result is derived. The relative field of attenuation by multiple flat-topped obstacles is solved in the similar way as that of a curvilinear-topped obstacle [P2].

Fig. 4 and Fig. 5 show the geometries for a curvilinear-topped obstacle and multiple flat-topped obstacles, respectively. For the curvilinear-topped obstacle shown in Fig. 4, the edges of the polygon should be long enough to satisfy the paraxial approximation in [19]. The field of attenuation relative to free space of multiple knife edges was solved in [1] and let us denote it as $\hat{E}(R)$. In [P2], the total field is given as the sum of 2^N field components for a curvilinear-topped obstacle with N reflection surfaces where the reflection coefficients can be regarded as constants. For example, if $N = 3$, the eight field components are derived to be as follows

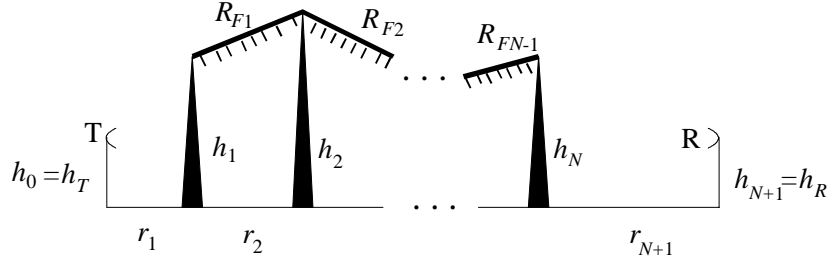


Fig. 4 Geometry for diffraction by a curvilinear-topped obstacle

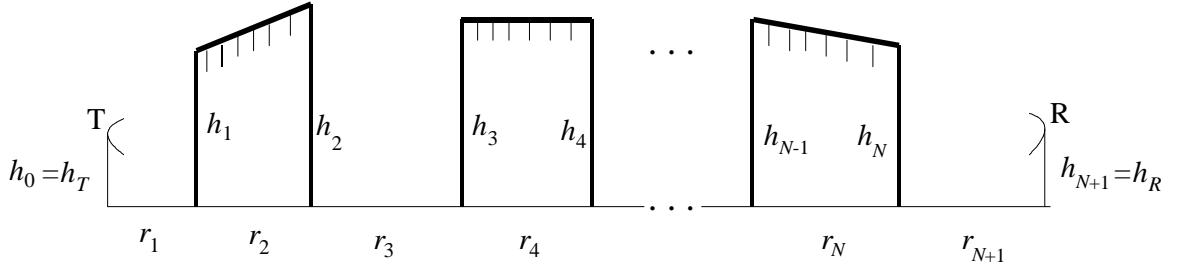


Fig. 5 Geometry for diffraction by multiple flat-topped obstacles

$$\hat{E}_1(R) = \hat{E}(R) = \hat{E}(\alpha_1, \alpha_2, \alpha_3) \quad (11a)$$

$$\hat{E}_2(R) = R_{F1} \cdot \hat{E}(-\alpha_1, \alpha_2, \alpha_3) \quad (11b)$$

$$\hat{E}_3(R) = R_{F2} \cdot \hat{E}(\alpha_1, -\alpha_2, \alpha_3) \quad (11c)$$

$$\hat{E}_4(R) = R_{F3} \cdot \hat{E}(\alpha_1, \alpha_2, -\alpha_3) \quad (11d)$$

$$\hat{E}_5(R) = R_{F1} R_{F2} \cdot \hat{E}(-\alpha_1, -\alpha_2, \alpha_3) \quad (11e)$$

$$\hat{E}_6(R) = R_{F2} R_{F3} \cdot \hat{E}(\alpha_1, -\alpha_2, -\alpha_3) \quad (11f)$$

$$\hat{E}_7(R) = R_{F1} R_{F3} \cdot \hat{E}(-\alpha_1, \alpha_2, -\alpha_3) \quad (11g)$$

$$\hat{E}_8(R) = R_{F1} R_{F2} R_{F3} \cdot \hat{E}(-\alpha_1, -\alpha_2, -\alpha_3) \quad (11h)$$

The definition of α_j ($j=1,2,3,\dots$) in (11) is available in [1], and the Vogler's multiple knife-edge field of attenuation $\hat{E}(R)$ includes the repeated integrals of the error function $I(n, \beta)$ which is expressed as

$$I(n, \beta) = \frac{2}{n! \sqrt{\pi}} \int_{\beta}^{\infty} (x - \beta)^n \exp(-x^2) dx \quad (12)$$

The solution of (12) can be found in [23]. For N multiple flat-topped obstacles, the total field is also the sum of 2^N field components, which have quite similar expressions as (11) and can be found in [P2].

3. MULTIPATH PROPAGATION STUDIES FOR TERRESTRIAL MICROWAVE COMMUNICATIONS

3.1 INTRODUCTION

The super-refractive layer formed in the lower atmosphere can completely reflect the radio wave in a terrestrial microwave communication link. This causes multipath propagation and may cause destructive interference at the receiving antenna. The multipath propagation causes frequency selective fading (FSF) which is regarded as in-band amplitude dispersion and it is the main factor of the quality degradation for medium and high capacity digital microwave communication systems [24][25]. The multipath propagation caused by an atmospheric duct is also one of the main factors of deterioration for cross-polarization discrimination (XPD) in dual polarized microwave communication systems [25][26].

3.2 THE ATMOSPHERIC DUCT AND THE METEOROLOGICAL CONDITION

An atmospheric duct means a layer, which can completely reflect the radio waves in lower atmosphere. The condition for the to formation of the atmospheric duct is that the refractive index gradients satisfy

$$dn/dz \leq -157 \times 10^{-6} / \text{km} \quad (13)$$

If we use the concept of refractivity $N = (n - 1) \times 10^6$, then the duct condition is

$$dN/dz \leq -157 N \text{ unit} / \text{km} \quad (14)$$

Eqs. (13) and (14) are for the spherical earth. If the plane earth case is considered, then the modified refractive index m and modified refractivity M should be introduced. The condition to form the atmospheric duct in the plane earth case is now as follows

$$dm/dz \leq 0 \quad (15)$$

$$dM/dz \leq 0 \quad (16)$$

The relationship between M and m is $M = (m - 1) \times 10^6$.

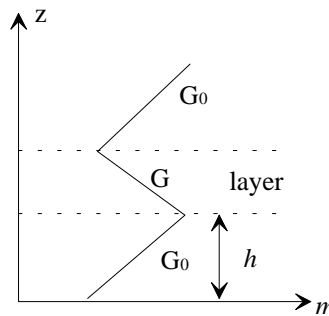


Fig. 6 Height profile of the modified refractive index

Fig. 6 shows how the modified refractive index changes with height. From this curve it is obviously seen that the atmospheric duct appears at the heights between h_1 and h_2 , because dm/dh is negative.

3.3 THE CUMULATIVE DISTRIBUTIONS FOR REFRACTIVE INDEX GRADIENTS IN LOWER ATMOSPHERE

The cumulative distribution of the refractive index gradient dn/dh in lower atmosphere changes with different seasons, regions and meteorological conditions. Based on data observed over many years, Yang et al. [27] showed that exponential and normal distributions have good agreement with the refractive index gradients inside and outside the layer, respectively. Therefore, inside the layer the cumulative distribution function (CDF) of the refractive index gradient G is

$$P(G' < G) = \frac{1}{2} \exp\left\{\frac{4(G-S)}{3V}\right\} \quad (17)$$

where parameters S and V can be fitted by using observed data. Outside the layer G_0 has the distribution

$$P(G' < G_0) = \frac{1}{2} \operatorname{erfc}\left\{\frac{G_0 - \bar{G}_0}{\sqrt{2}\sigma}\right\} \quad (18)$$

where \bar{G}_0 and σ are the mean value and standard deviation, respectively, which can also be derived from the observed data. The parameters S , V , 4 and 3 in (17), \bar{G}_0 and σ in (18) have no special meanings, they are just fitted or extracted from the measured data.

3.4 EXPERIMENTAL AND COMPUTER SIMULATION STUDIES OF FREQUENCY SELECTIVE FADING

3.4.1 Transfer function of multipath channel

In [P3], according to ray-based theory, the multipath power transfer function can be expressed as

$$P_r(f) = |H(f)|^2 = a_1^2 + a_2^2 + a_3^2 + 2a_1a_2 \sin(\omega\tau_2) - 2a_1a_3 \cos(\omega\tau_3) + 2a_2a_3 \sin[\omega(\tau_3 - \tau_2)] \quad (19)$$

where a_1 , a_2 and a_3 are the amplitudes for the direct, super-refractive and reflection rays, respectively.

In the frequency selective fading studies, the plane earth is considered here. Therefore, the modified refractive index and its gradient have been used in simulations. G and G_0 are the modified refractive index gradients outside and inside the layer, respectively. From (19), the

power transfer function of the channel is related to the delays and amplitudes of the rays. By using the ray tracing method, the excess delay is a function of G and G_0 for the super-refractive ray and function of G_0 for both direct and reflected rays [P3].

The normalized radiation pattern of the parabolic antenna used in this thesis is [28]

$$F(\theta) = (1 + \cos\theta) \frac{J_1(\pi D_A \sin\theta/\lambda)}{\pi D_A \sin\theta/\lambda} \quad (20)$$

where D_A is the aperture diameter, θ is off-axis angle and $J_1(\cdot)$ is the Bessel function of the first kind. The amplitude of the direct ray is set to unity, so the amplitudes of the super-refractive and reflected rays are

$$a_2 = F(\theta_0^T - \alpha_T) \cdot F(\theta_0^R - \alpha_R) \quad (21)$$

and

$$a_3 = R_e \cdot F(\theta_e^T - \alpha_T) \cdot F(\theta_e^R - \alpha_R) \quad (22)$$

where α_T and α_R , θ_0^T and θ_0^R , θ_e^T and θ_e^R are the transmitting and receiving angles of the direct, super-refractive and reflected rays, respectively, and they are functions of G and G_0 or G_0 [P3]. R_e is the effective ground reflection coefficient, which is affected by the spreading factor of the earth and the roughness ρ_s of the ground [29]. ρ_s is calculated by

$$\rho_s = I_0(\zeta) \exp(-\zeta) \approx \frac{1}{\sqrt{3.2\zeta - 2 + \sqrt{(3.2\zeta)^2 - 7\zeta + 9}}} \quad (23)$$

$$\zeta = \frac{8\pi^2 \sigma_h^2 \sin^2 \varphi}{\lambda^2} \quad (24)$$

Here $I_0(\cdot)$ is zero order modified Bessel function, σ_h is standard deviation of the ground roughness in the first Fresnel region near the mirror reflection point, and φ is angle between incident ray and ground.

3.4.2 Computer simulation method

The excess delays and amplitudes in (19) are functions of G and G_0 or G_0 , which are random variables with distributions given by Eqs. (17) and (18), and the samples of G and G_0 can be generated by the following equations

$$G = \frac{3}{4} \ln(2RW) \cdot V + S \quad (25)$$

$$G_0 = \sqrt{-2 \ln R_1} \cos(2\pi R_2) \cdot \sigma + \bar{G}_0 \quad (26)$$

where $W = 1/2 \cdot \exp(-4S/3V)$ and R , R_1 and R_2 are uniformly distributed random numbers in $[0,1]$. Let us assume that the center frequency and the bandwidth of the microwave link are f_0 and Δf , respectively. Depending on the bandwidth and center frequency, the odd number of the narrow band channels are assigned during the simulation and let $f_1, f_2 \dots, f_n$ denote the center frequencies of the narrow band signals. The flow chart of the computer simulation is shown in Fig. 7, where Z_h , Z_l and Z are the in-band dispersions for the upper and lower antennas and for diversity reception, respectively. In the simulation, five narrow band channels are used corresponding to the channels in the experiments.

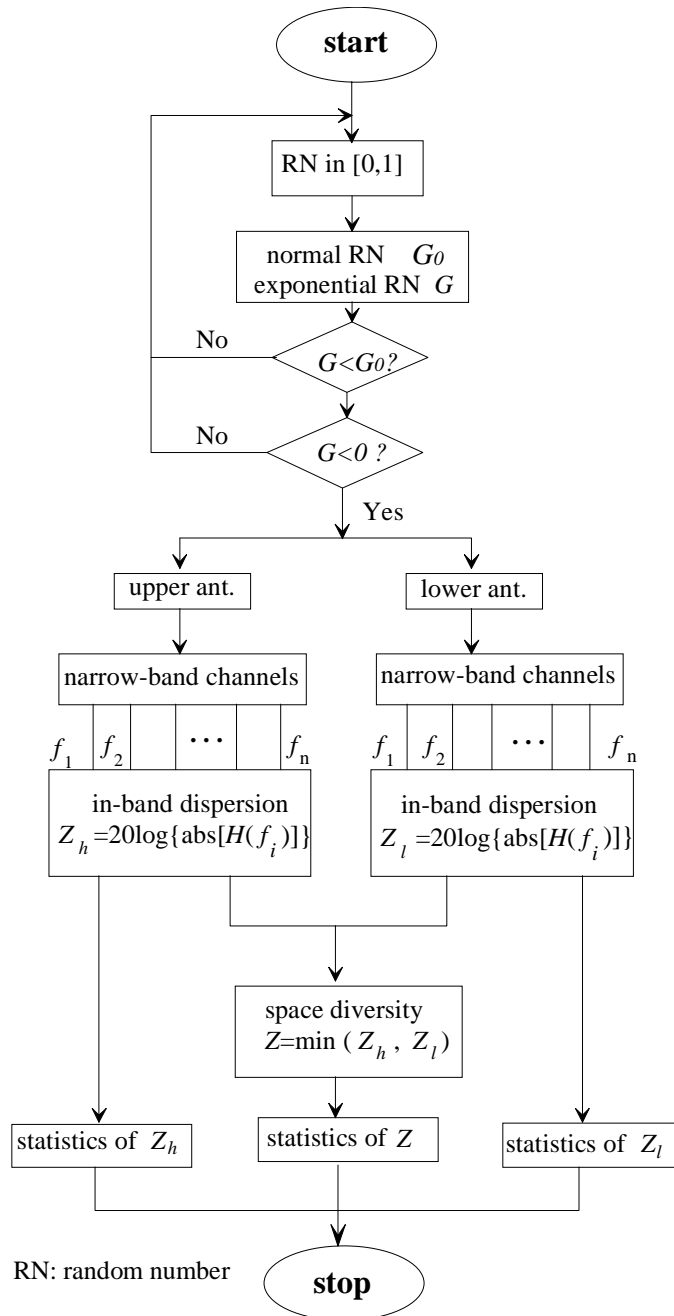


Fig. 7 Flow chart of the computer simulation

3.4.3 Measurement setup

The measurement setup is shown in Figs. 8(a) and 8(b). The signal is received by using frequency conversion to the intermediate frequency amplifier (IFA). The IFA has two outputs: one goes to A/D conversion and finally to the computer for detecting flat fading. Another output goes to a narrow-band receiver, whose five narrow-band signal outputs at different frequencies are stored by the computer. The main parameters of the narrow band receiver are: number of channels 5; center frequencies 57.7, 64.7, 70, 75.7 and 81.9 MHz; frequency interval 5.3 ~ 7 MHz; bandwidth 15 ~ 20 kHz; dynamic range 40 dB; channel isolation ≥ 50 dB and measurement accuracy 1 dB.

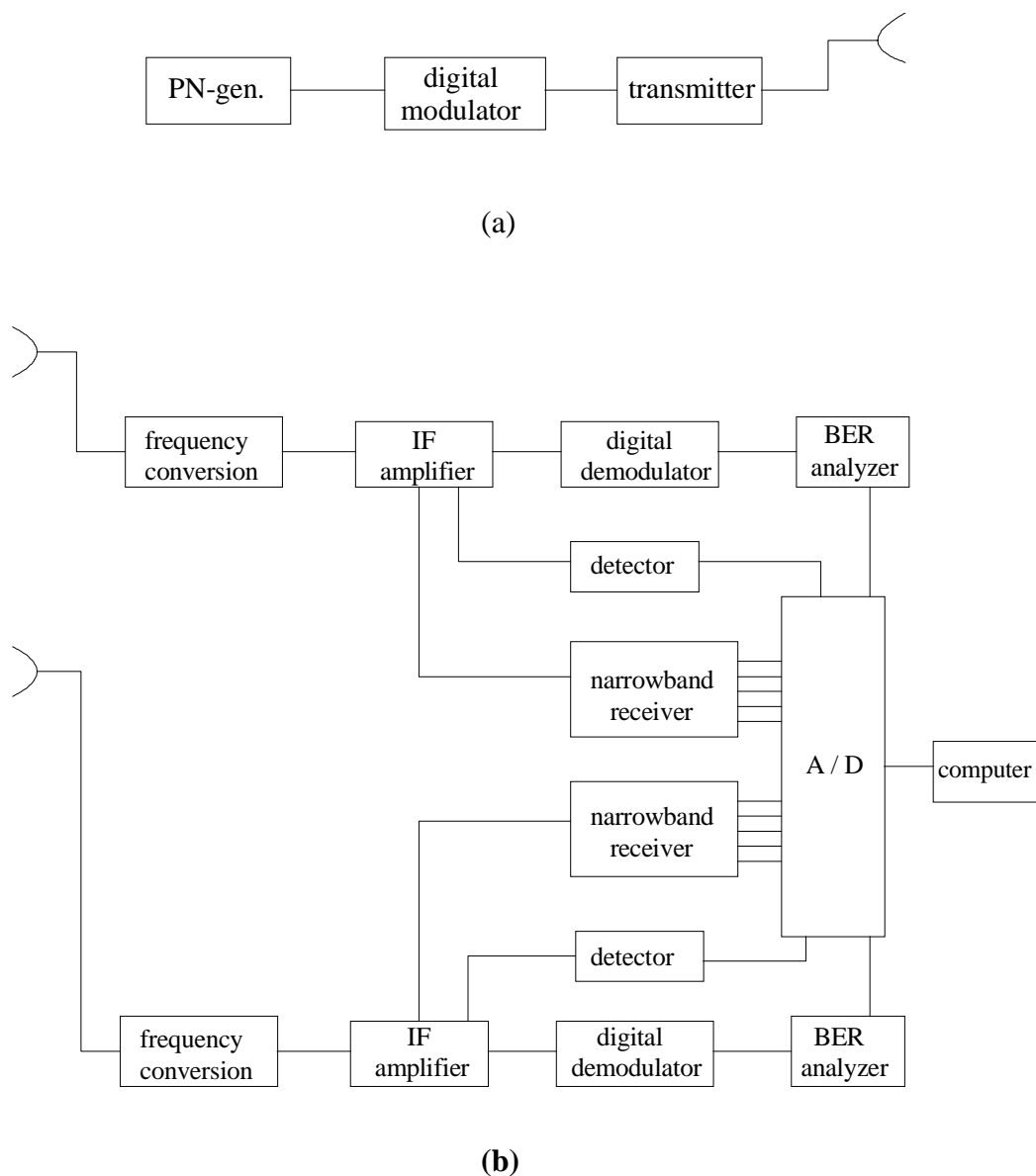


Fig. 8 The measurement setup. (a) The transmitting system. (b) The receiving system.

3.5 COMPUTER SIMULATION STUDIES OF DEPOLARIZATION DUE TO CLEAR AIR

As seen in Fig. 9, the spherical earth and a two-ray multipath model (direct and super-refractive rays) is considered for computer simulation of depolarization due to clear air [P4]. Assume that g and g_0 are the refractive index gradients for inside and outside of the layer. The factors K and K_0 of the earth's effective radii inside and outside the layer are

$$K = 1/(1 + r_0 g), \quad K_0 = 1/(1 + r_0 g_0) \quad (27)$$

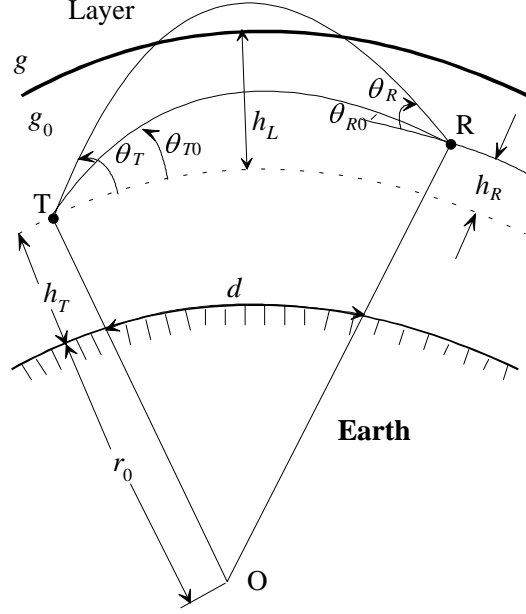


Fig. 9 The multipath rays in the spherical earth

where r_0 is the radius of the earth. The phase difference $\Delta\phi$ [26] between the super-refractive and direct rays can be calculated as

$$\frac{\lambda\Delta\phi}{2\pi n_t} = \frac{d^3}{24K_0^2 r_T^2} \left[3k^2 - 2k^3 - 1 + \frac{2(k-1)^3}{(1-K/K_0)^2} \right] + \frac{h_R^2}{2k^2 d} (1-k)^2 \quad (28)$$

where d and h_R are the distance and the height difference between transmitting and receiving antennas (when taking the transmitting antenna as the reference), respectively, $r_T = r_0 + h_T$ where h_T is the height of transmitting antenna from the ground, and n_t is the refractive index at the transmitting point. In (28), the parameter k satisfies the following quadratic equation [26]

$$\frac{k^4 d^2 [1 - (1 - K/K_0)^2]}{4K_0^2 r_T^2 (1 - K/K_0)^2} - \frac{k^3 d^2}{2K_0^2 r_T^2 (1 - K/K_0)^2} + k^2 \left[\frac{h_R}{K_0 r_T} - \frac{2h_L}{K_0 r_T} + \frac{d^2}{4K_0^2 r_T^2 (1 - K/K_0)^2} \right] - \frac{h_R^2}{d^2} = 0 \quad (29)$$

where h_L is the height of the lower boundary of the layer above the transmitting point. Assume that the cross polarization pattern of an antenna is [26]

$$f^2(\theta) = \begin{cases} f^2(0)\exp(c_x\theta^2) & |\theta| < |\theta_c| \\ f^2(0)\exp(c_x\theta_c^2) & |\theta| > |\theta_c| \end{cases} \quad (30)$$

where θ is the polar angle relative to the axis of the antenna, and c_x and θ_c are constants which can be fitted by using the measured cross polarization pattern of the antenna. The static cross-polarization discrimination is defined as

$$\text{XPD}_0 = -20\log_{10}\{2f(0)\} \quad (31)$$

In (30), the $f(0)$ can be derived from (31). The cross polarization discrimination (XPD) can be calculated as [26]

$$\begin{aligned} \text{XPD} &= 10\log_{10}\left\{\frac{2(1+\cos\Delta\varphi)}{f^2(0)\left[\exp(c_x(\theta_R-\theta_{R0})^2)+2\exp(0.5c_x[(\theta_R-\theta_{R0})^2+(\theta_T-\theta_{T0})^2])+\exp(c_x(\theta_T-\theta_{T0})^2)\right]}\right\} \\ &= \mathcal{F}(\Delta\varphi, f(0), \theta_R, \theta_{R0}, \theta_T, \theta_{T0}, c_x, \theta_c) \quad \left|\theta_T - \theta_{T0}\right| \text{ and } \left|\theta_R - \theta_{R0}\right| < \left|\theta_c\right| \end{aligned} \quad (32)$$

where θ_{T0} and θ_{R0} , and θ_T and θ_R are the transmitting and receiving angles for both the direct and super-refractive rays, respectively. When $|\theta_T - \theta_{T0}|$ and $|\theta_R - \theta_{R0}|$ are in the other intervals shown in [P4], the XPD can also be calculated by changing the parameters in the function \mathcal{F} . The co-polarized attenuation (CPA) is calculated as

$$\text{CPA} = -10\log_{10}[2(1+\cos\Delta\varphi)] \quad (33)$$

From (28), (32) and (33), it is seen that XPD and CPA are functions of the factors of the earth's effective radii K and K_0 , namely XPD and CPA change with the refractive index gradients g and g_0 inside and outside the layer. The distributions and the sample generation for g and g_0 are similar in Sections 3.3 and 3.4.2. By using (32) and (33), the statistical distributions of XPD and CPA can be obtained by computer simulations.

The simulation and experimental studies of depolarization due to multipath propagation in [P4][30] show that the equal probability values of XPD and CPA have a linear relationship. The slope is within $(-1, 0)$ and not always equal to -1 as suggested by ITU-R recommendation [31]. This linear relation enables us to introduce a simple and valuable method for predicting XPD based on the prediction of CPA.

4. PROPAGATION CHARACTERIZATION OF RADIO CHANNELS FOR FUTURE WLAN MOBILE COMMUNICATION SYSTEMS

4.1 INTRODUCTION

It has been of great interest in wireless broadband communications in recent years to meet the demand of communication capacities. The wireless local area network (WLAN) is directed to communication between computers, of which HIPERLAN (high performance LAN) Types 1 and 2, [32][33] and IEEE 802.11 [34] are examples. The frequency band 5.15-5.30 GHz has been ratified for HIPERLAN use by the Conference of European Postal and Telecommunications Administrations (CEPT) [35].

HIPERLAN Type 1 is a WLAN standard designed to provide high-speed communications (20 Mbit/s) between portable devices. It is intended to allow flexible wireless data networks to be created without the need for an existing wired infrastructure and it can be used as an extension of a wired LAN. HIPERLAN Type 2 is intended for complementary access mechanism for universal mobile telecommunication systems (UMTS) as well as for private use as a wireless LAN. It will offer higher-speed access (54 Mbit/s) to a variety of networks including the UMTS core networks, the asynchronous transfer mode (ATM) networks and the internet protocol (IP) based networks. Such a high transmission rate will be achieved by using orthogonal frequency division multiplexing (OFDM) modulation method, which is particularly efficient in time dispersive environments.

WLAN environments are quite complicated, the radio channel has severe delay dispersion resulted from multipath propagation. The delay dispersion will cause intersymbol interference (ISI) which limits the data rate. Therefore, a basic understanding of the channel is quite important for finding better modulation and coding schemes and for designing equalizers that improve the channel. Radio propagation information is also quite important for analyzing and/or designing radio coverage and interference of WLAN systems. Due to complicated mobile radio environments, theoretical prediction methods are not accurate enough to characterize the mobile radio channel. In this thesis, different mobile environments have been measured at 5.3 GHz using the wideband channel sounder developed at the IDC of HUT [3][4].

4.2 BASIC PROPAGATION CONCEPTS AND MODELLING PARAMETERS

In mobile radio systems, two main radio channel issues are considered in this thesis: link budget and delay dispersion. The link budget is determined by the amount of received power that may be expected at a particular distance or location from a transmitter, and it determines some fundamental quantities such as required transmit power, coverage areas, and battery life. Delay dispersion arises due to multipath propagation whereby replicas of the transmitting signal reach the receiver with different propagation delays. The delay dispersive nature of the channel determines the maximum data rate that may be transmitted without requiring an equalizer [2].

Small scale and large scale fading: Due to multipath propagation, when a mobile moves over short distances, the instantaneous received signal strength fluctuates rapidly giving rise to small scale fading. As the mobile moves away from transmitter, the local average of the received signal will decrease gradually. For the macro-cellular case, it was proven in [36] that 20 to 40 λ (wavelength) is most suitable window length or sector length to average fast fading components. For the micro-cellular case at 900 MHz, 5 λ (about 1.7 meters) has been shown feasible based on measurements [37]. At 5.3 GHz, it is shown in this thesis that 20 – 40 λ (about 1.1 – 2.3 meters) is the best window lengths based on large amount of measured data in outdoor and indoor environments [P5][P6]. Therefore, it is recommended that the practical window length for averaging small scale fading is 1 – 2 meters in micro- and pico-cells at 900 MHz – 5 GHz frequency bands. In [P5], the boundaries of the window length were empirical and based on the comparisons of the minimized standard deviations, however, the upper boundary cannot be more than 40 λ .

Path loss: Path loss is an important parameter for not only predicting the coverage area, but also for predicting the interference signals that a user will experience from other RF sources. Path loss can be derived by using the following formula to fit the measured data [38][39][P6]

$$PL(d) = PL_0(d_0) + 10n \log_{10}(d/d_0) + X_\sigma \quad (34)$$

This is called lognormal shadowing path loss model, where n is the path loss exponent, d_0 is the reference distance which should always be in the far field of an antenna in free space. d is the distance from the transmitter to receiver and X_σ is zero mean Gaussian random variable with standard deviation (STD) σ . Typically, d_0 equals 1 km for large urban mobile systems, 100 m or 1 m for micro-cellular systems [38].

The empirical path loss models can also be derived by using a two-parameter (both n and PL_0 are variables) least square method [40]-[42][P5],

$$PL(d) = PL_0 + 10n \log_{10} d \quad (35)$$

where there is no reference distance and d is in meters. In semi-log coordinates, PL_0 is the intercept point at the vertical axis and n is the slope.

The least square method has been applied in the path loss models shown in (34) and (35) when deriving the empirical path loss models from measured data. In (34), the reference free space distance d_0 should be decided first when using the models. However, the mobile environments are quite complicated and it is hard to know what d_0 exactly is for a specific environment. The same reference distance for all macrocells or microcells is obviously not quite reasonable. Therefore, in practical applications, (35) can give better fit to measured data with lower STD [P5].

In order to reduce the fitted STD when using (34) and (35), line-of-sight (LOS) and non-line-of-sight (NLOS) situations should be distinguished. In the LOS case, the break point should be noticed, because at it the path loss exponent changes a lot. The distance of the break point from

the base station is approximately equals to $4h_M h_B / \lambda$, where h_M and h_B are the antennas heights for the mobile and base station from ground level [43].

The path loss model for multiple floors and multiple walls (Motley Keenan model) is also available in [44]. The path loss is strongly dependent on the structures and not a linear function of the numbers of the walls and floors.

Guided wave effect: In many LOS corridors and street canyons, the received power is found to be higher than that in free space in [P5][P6] and also in [38][39]. This phenomenon is called guided wave effect. Due to the fact that the energy of the propagating waves is confined in the waveguides, so it cannot spread in every direction like in free space. In such corridors and street canyons, some dominant propagation models are existed, and they depend on the dimensions of the waveguides and the frequency bands of propagating waves.

Delay spread: Mobile radio channel has delay dispersion due to multipath propagation. Because the multipath propagation is dependent upon the geometric relationships between transmitter and receiver, and the surrounding physical environment, the delay dispersion appears random. Therefore, statistical parameters such as mean excess delay and rms delay spread etc. are often considered. In delay domain, the power delay profile, which is a function of excess delay, and average received power can be measured by a channel sounder. The mean excess delay is the first central moment of the power delay profile and rms delay spread is the standard deviation of the excess delays. The rms delay spread is a most important modelling parameter which is connected to the capacity and the bit-error-rate (BER) of a specific communication system and the complexity of a receiver. Results in [45][46] show that the error floor is approximately proportional to the square of the normalized rms delay spread, namely the BER is equal to $K \cdot (S/T)^2$, where the proportionality constant K depends on the modulation format, the filtering at the transmitter and receiver, and the sampling time, S is the rms delay spread and T is the symbol duration. This dependency between BER and rms delay spread is true, however, only under some special assumptions [47][48]: The maximum excess delay of the channel must be much smaller than the symbol length, and the channel must be Rayleigh fading. For a given BER, by comparing the rms delay spread and the symbol duration, one can determine if any equalizer is required in the receiver.

Spatial and frequency correlations: Spatial and frequency correlation studies are useful for the design of antenna diversity to reduce multipath fading. The formulas for calculating spatial and frequency correlation functions can be found in [49][P6]. Because the correlation behaviour is a small scale effect, the wide sense stationary uncorrelated scattering (WSSUS) should be assumed. To meet this condition, 100 - 200 IRs (about 20 - 40 wavelengths) are used as the window length to calculate the correlation functions and finally an average correlation function can be obtained. In this thesis, envelope correlation is considered for narrowband signals. However, recent research [50] has shown that spatial correlation characteristics do not largely depend on frequency bandwidth up to approximately 20% of the carrier frequency. Therefore, the narrowband model is sufficient for calculating the signal correlation characteristics within $B \leq 0.2f_c$, where B is the bandwidth of a transmitted signal and f_c is the carrier frequency. At 5.3 GHz, the studies in [P5] show that the correlation is strongly dependent on the transmitter height and LOS and NLOS situations in different environments.

Path number distribution: Poisson's and modified Poisson's distributions were considered for the multipath number in [51]. Modified Poisson's distribution was shown to have good agreement with the experiment results in some cases. However, modified Poisson's distribution does not have an explicit expression, but is just a process. Therefore, it's not convenient for practical use. In [52][53], another simple and useful path number distribution was introduced by considering the path number variation of radio waves in land mobile communications to be a Markov process at finite state space, and it was shown to have good agreement with the experimental results. The path number distributions given by Poisson and Gao [52][53] can be expressed as

$$P(N) = \frac{\eta^{N_T - N}}{(N_T - N)!} e^{-\eta} \quad (36)$$

$$P(N) = C_{N_T}^N \frac{\eta^{N_T - N}}{(1 + \eta)^{N_T}} \quad (37)$$

where N is a variable, C means combination, and the maximum number of paths that mobile can receive is N_T . The parameters η and N_T can be found by fitting into the experimental data. For Poisson's probability density function (PDF), the mean path number is $\langle N \rangle = \eta$. For Gao's PDF, the mean value is $\langle N \rangle = N_T / (1 + \eta)$. It is shown in [P5] that both Poisson's and Gao's PDFs have good agreement with the experiment results. However, Gao's PDF has better fit especially at high probability values. In [P5], the path numbers are obtained by counting the peak values in the PDPs, however, some other methods such as CLEAN algorithm [54] might be used in further studies.

Amplitude distribution and Ricean K -factor: There are several amplitude distributions such as Rice, Rayleigh, Nakagami (also called m -distribution), lognormal and Suzuki distributions [55] to describe both narrowband and wideband signals. The Nakagami distribution contains many other distributions as special cases. The Suzuki distribution is a mixture of Rayleigh and lognormal distributions. The lognormal distribution has often been used to explain large scale variations of the signal amplitudes in a multipath environment. For wideband radio channel studies at 5.3 GHz in this thesis, Rice and Rayleigh distributions are proven to be the best to characterize the envelope amplitude. A well accepted model for small scale rapid amplitude fluctuations in absence of a strong received component is the Rayleigh fading. However, when a strong path exists in addition to the lower level scattered paths, Ricean fading appears. This strong components may be a LOS path or a path that goes through much less attenuation compared to other arriving components. The Rice distribution can be characterized by Ricean factor which is defined as follows

$$K = s^2 / 2\sigma^2 \quad (38)$$

where σ^2 is average fading power of the non-dominant paths and s is the peak amplitude of the dominant received multipath component. There are several methods for estimating K -factor from measured data [56]-[59]: method of least square, moment method (MoM) and method of maximum likelihood (ML). The least square method is a traditional method which

directly uses measured data to fit Rice distribution while the standard deviation is minimized. There are two formulas based on MoM which can give a quick estimation of the K -factor called μ -based method and γ -based method [57]

$$\mu = \frac{\sqrt{\pi}}{2} (K+1)^{-1/2} \exp(-K/2) \cdot [(K+1)I_0(K/2) + KI_1(K/2)] \quad (39)$$

$$\gamma = \frac{2K+1}{(K+1)^2} \quad (40)$$

where $\mu = E[A] / \sqrt{E[A^2]}$ and $\gamma = V[A^2] / (E[A^2])^2$ with $E[.]$ denoting the expected value and $V[.]$ the variance. A is the received signal envelope. Eqs. (39) and (40) are quite simple for practical use. However, the studies in [57] show that for low mobile speed which introduces significant correlation among signal samples, the estimators' performance becomes deteriorated due to the reduction in the number of independent samples. In this thesis, the least square method has been applied [P6][P7].

4.3 TAPPED DELAY LINE CHANNEL MODELS

The following parameters should be specified when developing a tapped-delay-line channel (TDL) model [60][P6][P7]

- Number of taps
- Excess delays of the taps
- Relative amplitudes of the taps
- Amplitude distributions of the taps
- Doppler spectra of the taps
- Correlation between consecutive taps

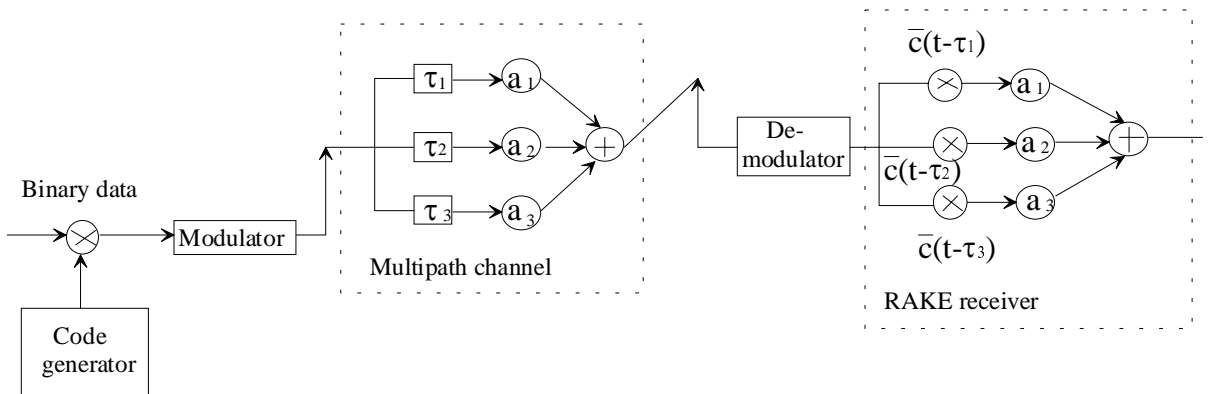


Fig. 10 Principle of RAKE receiver [61].

When a TDL model is developed, it gives the radio channel transfer function. Therefore, some anti-fading measures can be adopted, e.g. using an equalizer or a RAKE receiver shown in Fig.

10. The RAKE receiver consists of correlators, each receiving a multipath signal. After despreading by correlators, the signals are combined using, for example, maximal ratio combining.

In [P6] and [P7], based on some basic theories introduced in [60], tapped-delay-line (TDL) models for indoor and outdoor mobile communications are developed for the first time at 5.3 GHz frequency band. The TDL models with 4, 5 and 6 taps are considered. For an equalizer, 4 or 5 taps seems currently the maximum which is practically realizable [48].

4.4 PROPAGATION MECHANISM STUDIES FOR DIFFERENT TYPES OF DOPPLER SPECTRA

Considering Doppler spectrum studies, important models were presented by Clarke [62] and Aulin [63] which are typical 2- and 3-D models, respectively. It has been shown that 3-D Doppler spectra are suitable to describe indoor as well as outdoor mobile communications when base station antenna height is over rooftop [64]. In this case the Aulin, Gaussian, Laplacian, double-sided exponential and other PDF models have been used to describe the angles of arrival (AoAs) of the scattered waves in the elevation plane [63]-[67]. In both 2- and 3-D cases, it is often assumed that the AoAs of the scattered waves in the azimuth plane are uniformly distributed in $[0, 2\pi)$. However, in some practical propagation environments [68], the AoAs have been found to be distributed in an arbitrary angular range $[\alpha_1, \alpha_2]$. Meanwhile in the elevation plane, the AoAs can also be assumed to be distributed in another arbitrary angular range $[\beta_1, \beta_2]$. In some papers [61][69][P6], the names of Doppler spectra have been given, but there is some lack in explaining the physical background in terms of propagation mechanisms for more general AoAs distributions in the azimuth and elevation planes.

4.4.1 Formulation of theoretical Doppler spectrum modelling

Assume that mobile radio channels are WSSUS and a mobile terminal is moving along a straight line in xy-plane as shown in Fig. 11. In [P7], an autocorrelation function is derived as

$$R(\tau) = \int \int_{\alpha \beta} P_{\alpha}(\alpha) \cdot g_{\alpha}(\alpha) \cdot P_{\beta}(\beta) \cdot g_{\beta}(\beta) \cdot d\alpha d\beta \cdot \exp[jk \cdot v \cdot \tau \cdot \cos(\alpha - \gamma) \cdot \cos \beta] \quad (41)$$

where $P_{\alpha}(\alpha)$ and $P_{\beta}(\beta)$ are the PDFs of the AoAs of the scattered waves in the azimuth and elevation planes, respectively, and $g_{\alpha}(\alpha)$ and $g_{\beta}(\beta)$ are normalized antenna radiation patterns in the planes. The definition of angles α_l and β_l for l -th multipath ray is shown in Fig. 11. The 2-D and 3-D autocorrelation functions can be derived from (41) by assuming that the mobile moves along x-axis ($\gamma = 0$) for simplicity. By applying Fourier transformation to the autocorrelation function, the corresponding Doppler spectral density is obtained by

$$S(f_D) = \int_{-\infty}^{\infty} R(\tau) \exp(-j2\pi \cdot f_D \tau) d\tau \quad (42)$$

where f_D is the Doppler shift.

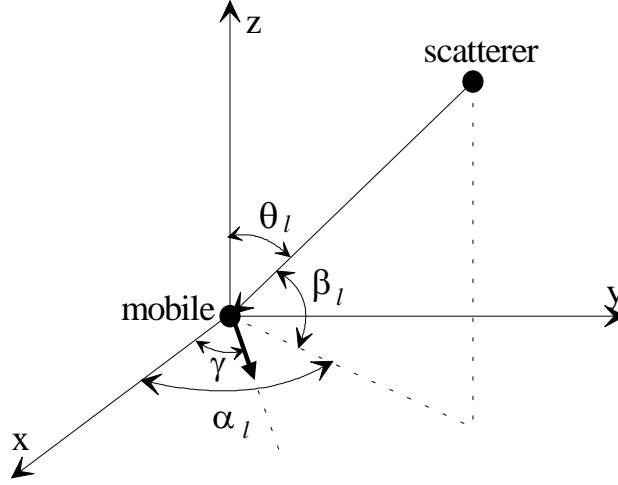


Fig. 11 Geometry for a 3-D scattered environment

4.4.2 Empirical Doppler Spectrum modelling

Empirical Doppler spectra are derived in [P6][P7] using the delay Doppler function or scattering function $U(\tau, \gamma)$ [70]

$$U(\tau, \gamma) = \int_{-\infty}^{\infty} h(\tau, t) e^{-j2\pi\gamma t} dt \quad (43)$$

where γ denotes the Doppler frequency. The Doppler spectrum is due to small scale effect, so WSSUS radio channel should be assumed. This is satisfied by choosing sets of 100 IRs (about 1.1 meter) from the collected IRs to get instantaneous samples of the Doppler spectrum, and finally the average Doppler spectrum is obtained for a specific mobile environment.

4.5 A GENERAL COMPUTER SIMULATION METHOD FOR 3-D RECEIVED SIGNAL LEVEL IN WIDEBAND MOBILE COMMUNICATIONS

In this thesis, we extended the 2-D work shown in [71][72] to 3-D case under general and reasonable assumptions. These are that the path number has Poisson distribution, multipath amplitudes follow Rayleigh or Rice distribution, the AoAs in both of the azimuth and elevation planes follow uniform and Gaussian distribution, respectively, and excess delay follows exponential distribution. The 3-D received power for wideband signal was expressed as

$$P(\Delta f) = 2\Delta f \left\{ \sum_{i=1}^N A_i^2 + \sum_{i=1}^N \sum_{\substack{j=1 \\ j \neq i}}^N A_i A_j \cos(Kf_c \cdot \Delta L_{ij}) \text{sinc}(K \cdot \Delta f \cdot \Delta L_{ij}) \right\} \quad (44)$$

where $2\Delta f$ is the bandwidth of transmitted signal with carrier frequency f_c , A_i and A_j are the amplitudes of scattered waves, $K = 2\pi / c$ and c is the speed of light. Let us assume that the mobile is surrounded by scatterers and is moving along the x-axis with a speed v , as shown in Fig. 12. In the 3-D case, the path length difference can now be expressed as

$$\Delta L_{ij} = L_i - L_j - vt \cdot (\cos \psi_i - \cos \psi_j) = L_i - L_j - vt \cdot (\cos \theta_i \cos \phi_i - \cos \theta_j \cos \phi_j) \quad (45)$$

where L_i and L_j are path lengths for the i -th and the j -th waves at the starting point O, respectively [72], and $t = n\Delta t$ (Δt is the time step). In (45), let us define

$$L_{ij} = L_i - L_j = c \{ (L_i/c - L_{\min}/c) - (L_j/c - L_{\min}/c) \} = c(\tau_i - \tau_j) \quad (46)$$

where L_{\min} is the minimum path length, τ_i and τ_j are excess delays for the i -th and j -th waves. Fig. 13 presents the flow chart of the simulation performed in this work.

The input parameters of the simulation and simulation results are available in [P8] for wideband and narrowband received signal levels. Severe time selective fading can be observed for wideband received signal when signal amplitudes follow Rayleigh distribution.

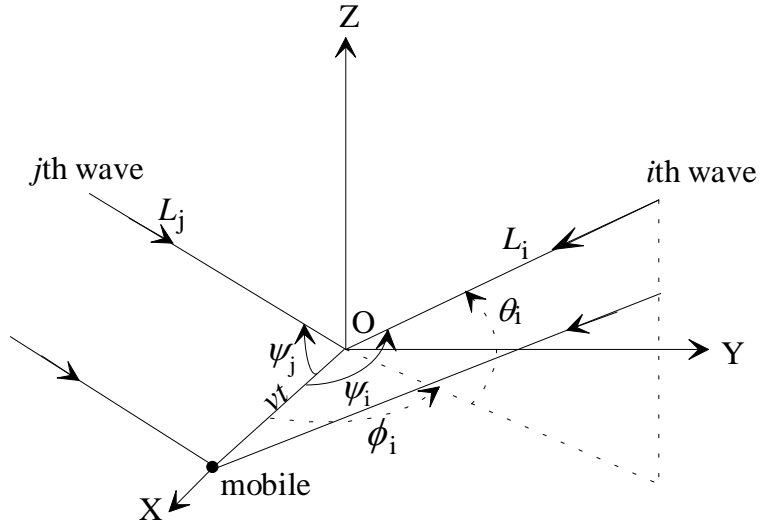


Fig. 12 Geometry of 3-D propagation

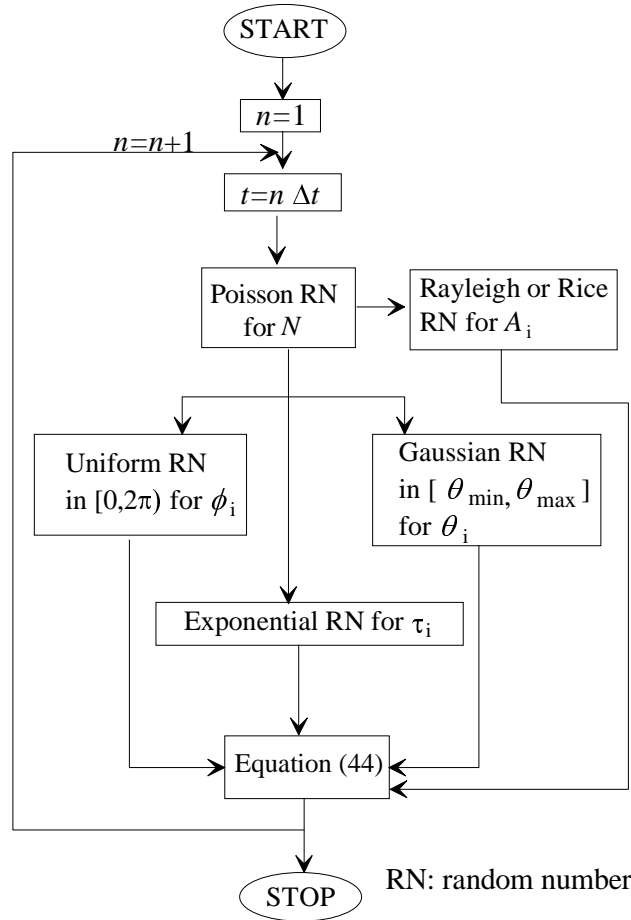


Fig. 13 Flow chart of the computer simulation

5. SUMMARY OF PUBLICATIONS

In [P1], a general formula of the attenuation by multiple knife edges with ground reflections is derived and further the field of attenuation for double knife edges with ground reflections is solved for the first time in the paper by using physical optics. The total field includes eight field components, but the number of these components can be reduced by locating the main reflection point. The fluctuation of the received field in the illumination region is due to the reflection from the region at where the main reflection point is located. The received field fluctuation in the diffraction region is due to the reflection from the area between the last knife edge and the receiver.

In [P2], by using physical optics and implementing complicated integral transformations, attenuations by curvilinear-topped obstacles and multiple flat-topped obstacles are solved by summing 2^N field components, where N is the number of the curvilinear lines or flat-topped obstacles. The results derived are the simplest and easiest ones presented for practical use. To calculate the field components one just needs to change the signs of $\alpha_j (j=1,2,3,\dots)$ in Vogler's formula for the attenuation by multiple knife edges.

In [P3], a novel simulation method is introduced and applied to frequency selective fading by using a three-ray multipath model with the assumption of a plane earth. Based on measurements and simulations, flat fading, in-band dispersion and space diversity effect are studied in detail. The excess delays and the amplitudes of the rays are derived as functions of the modified super-refractive index gradients inside and outside the layer. The gradients are random variables which form the basis of simulation. The correlation between flat fading and in-band dispersion is also studied, which offers an effective way to predict in-band dispersion using flat fading.

A similar simulation method compared to the method introduced in [P3] is also applied in [P4] to study the depolarization effects due to clear air by using a two-ray multipath model with a spherical earth. Based on some formulas derived in [26] and [P4], the statistical distributions of cross-polarization discrimination and co-polarized attenuation, and the relationship of their equiprobability values are simulated.

In [P5] and [P6], the latest propagation parameters and models are provided at 5 GHz. These are of great importance in designing future WLAN mobile communication systems. Especially the tapped-delay-line channel models are developed for the first time in this frequency band.

To get the results, in [P5], a large outdoor measurement campaign at 5.3 GHz was performed in Helsinki in 1999 with different base station heights in urban, suburban and rural environments. Based on the measured database, empirical or semi-empirical models and parameters are derived. These include path loss models, excess delay and rms delay spread, window length for averaging fast fading components, spatial and frequency correlations and path number distributions. Rotation measurements were also performed with a directive horn to study spatial propagation mechanisms and directions of arrival of multipath rays.

In [P6], empirical models are developed for typical office environments and one large hall with mainly omni-directional antennas at 5.3 GHz. Empirical models and parameters such as path loss models, tapped-delay-line channel models, rms delay spread, spatial and frequency correlations are developed/derived for indoor environments.

In [P7], a novel theoretical modelling method has been introduced to explain the physical backgrounds of measured Doppler spectra in 3-D scattered environments from propagation mechanism point of view. First, a general 3-D autocorrelation function is derived in a 3-D scattered environment with the assumption of WSSUS radio channel. It is related to the PDFs of the AoAs of the waves and antenna radiation patterns in both of the azimuth and elevation planes. By applying Fourier transformation to the autocorrelation function, the corresponding power spectral density can be obtained.

In [P8], a new and general method is introduced to simulate 3-D wideband received signal level in urban environments. Some distributions for the path number, amplitude, the AoAs in the azimuth and elevation planes and excess delay have been applied for simulation purpose. However, they can be replaced by more accurate and new research results of the distributions.

6. CONCLUSION

The analytical expressions for the fields of attenuation by some typical-shaped terrain obstacles are derived in this thesis. These can be applied in field strength predictions not only to terrestrial fixed and mobile communications, but also to some radar systems in frequency bands higher than VHF. The double knife-edge attenuation with ground reflections is solved for the first time in the case where the reflection coefficients can be regarded as constants. The fields of attenuation by curvilinear-topped obstacles and multiple flat-topped obstacles are also solved in closed forms, which are the simplest and easiest ones available at the moment for practical use.

Computer simulation is an effective way to study frequency selective fading and depolarization effects for terrestrial microwave links and dual polarized communication systems. In this work, novel simulation methods are introduced and applied to these research fields. It is illustrated that diversity reception reduces significantly flat fading and in-band dispersion. Fading and dispersion are severe during small percentage of time. The in-band linear amplitude dispersion, as well as the in-band maximal amplitude dispersion, have a relatively high correlation. The equiprobability values of in-band linear amplitude dispersion and flat fading depth have an excellent linear relationship with the slope less than unity. This linear relationship enables us to introduce a simple and useful method for predicting the frequency selective fading by means of the flat fading. In this thesis, the cross-polarization discrimination and co-polarized attenuation statistical distributions are also simulated due to clear air. The equiprobability values of the cross-polarization discrimination and co-polarized attenuation shown in the simulation and experiment have a linear relationship with slope within $(-1, 0)$ and does not always equal -1 as stated in ITU-R recommendation.

The latest modelling parameters and models are presented in this work for outdoor and indoor mobile communications at 5.3 GHz. The modelling results based on the outdoor measurements at 5.3 GHz show that the path loss exponents are within $1.4 - 3.5$ in LOS and $2.8 - 5.9$ in NLOS, respectively. The mean excess delay and mean rms delay spread are within $29 - 102$ ns and $22 - 88$ ns, respectively. Large excess delays of up to 1.2 μ s and rms delay spread of about 0.42 μ s were found in the urban rotation measurements. A suitable window length of $1 - 2$ m to average out fast fading components for micro- and pico-cells at 5 GHz frequency bands was found. The correlation distances at this frequency band with the correlation coefficient of 0.7 are between 1 and 11λ and the respective correlation bandwidths at 0.7 are between 1.2 and 11.5 MHz. These correlation values depend strongly on base station antenna heights. Both Poisson's and Gao's PDFs agree well with the experimental results of the path number distributions. However, Gao's PDF is shown to be better than Poisson's especially at high probability values.

The modelling results based on the indoor measurements at 5.3 GHz show that the path loss exponents are $1.3 - 1.5$ in LOS and $2.9 - 4.8$ in NLOS. Large difference in NLOS path loss exponents is due to different propagation mechanisms in different types of building structures. For the rms delay spread, the values for $CDF = 0.9$ vary from $20 - 180$ ns in different office buildings and in a large hall. Tapped-delay-line channel models are developed with four taps in the indoor cases. The taps in these models undergo Rayleigh fading except the first one, which typically shows a small Ricean factor in LOS cases. This shows that even in the LOS case the energy of scattered waves is significant.

The Doppler spectra observed in the measurements are defined and the physical reasons are explained for the first time in this work from propagation point of view for 3-D scattering environments. The “narrow” spectrum arises when the scattering is over a narrow range of angles in azimuth plane. This might be because there is a wave coming directly from the transmitter, and it dominates over the scattered waves. In this case the envelope amplitude pdf will be Ricean. But, on the other hand, the scattering may be over a narrow range of angles without a significant direct component, in which case the amplitude will be Rayleigh distributed. The “flat” spectrum occurs in the idealized situation when both the scattering and the receiver’s antenna are isotropic in three dimensions. The dip between the two horns of the isotropic 2-D spectrum is filled in as more scattering comes from directions other than the purely horizontal. There is no predominant direct wave from the transmitter, and hence the envelope amplitude is Rayleigh distributed.

Severe time selective fading can be observed when multipath amplitudes follow Rayleigh distribution for 3-D wideband received signal in urban environments. However, the fading margin is significantly reduced when the amplitudes follow Rice distribution with higher Ricean factor. Such simulation can provide detailed fading characteristics for a specific urban environment.

ERRATA:

[P3]: In the first two equations of Eq. (14), Δh should read $\Delta h/d$. In the first line of Section 3.3, directivity should read radiation pattern. In the line below Eq. (23), $W = \exp(-4S/3V)$ should read $W = 1/2 \cdot \exp(-4S/3V)$.

[P4]: In Section 1 and line 3, co-polar discrimination should read cross-polarization discrimination. In Eq. (3), $f(\theta)$ should read $f^2(\theta)$. In Eqs. (5) and (6), F should read \mathcal{F} . In line 2 below Eq. (8), N/km should read 1/km. In Eq. (10), $2k^2$ should read $2k^3$. In Eq. (15), the last term should read $-h_R/kd$. In the line below Eq. (19), $W = \exp(-4s/3v)$ should read $W = 1/2 \cdot \exp(-4s/3v)$.

[P5]: Delete $d_0 = 1$ m in the line below Eq. (2).

[P8]: In Section 2 and the 5th assumption, $\exp(\tau/T)/T$ should read $\exp(-\tau/T)/T$. In Section 6, line 5, frequency-selective should read time-selective. In Section 7 and line 3, in Table 1, and in the caption of Fig. 3, Rician should read Ricean.

REFERENCES

- [1] L. E. Vogler, "An attenuation function for multiple knife-edge diffraction," *Radio Sci.*, vol. 17, no. 6, pp. 1541-1546, Nov.-Dec. 1982.
- [2] J. Bach. Andersen, T. S. Rappaport, and S. Yoshida, "Propagation measurements and models for wireless communications channels," *IEEE Commun. Magazine*, vol. 33, no. 1, pp. 42-49, Jan. 1995.
- [3] J. Kivinen, *Development of Wideband Radio Channel Measurement and Modelling Techniques for Future Radio Systems*, Doctor Thesis, Helsinki University of Technology, 2001.
- [4] J. Kivinen et al., "Wideband radio channel measurement system at 2 GHz," *IEEE Trans. Instrum. Meas.*, vol. 48, no. 1, pp. 39-44, Feb. 1999.
- [5] P. D. Holm, "UTD-diffraction coefficient for higher order wedge diffracted fields," *IEEE Trans. Antennas Propagat.*, vol. 44, no. 6, pp. 879-888, June 1996.
- [6] D. A. McNamara, C. W. I. Pistorius, and J. A. G. Malherbe, *Introduction to the Uniform Geometrical Theory of Diffraction*, Norwood, MA: Artech House, 1990.
- [7] J. B. Keller, "Geometrical theory of diffraction," *J. Opt. Soc. Amer.*, vol. 52, no.2, pp.116-130, Feb. 1962.
- [8] R. G. Kouyoumjian and P. H. Pathak, "A uniform geometrical theory of diffraction for an edge in a perfectly conducting surface," *Proc. IEEE*, vol. 62, no.11, pp.1448-1461, Nov. 1974.
- [9] P. D. Holm, "A new heuristic UTD diffraction coefficient for nonperfectly conducting wedges," *IEEE Trans. Antennas Propagat.*, vol. 48, no. 8, pp. 1211-1219, Aug. 2000.
- [10] K. R. Jakobsen, "An alternative diffraction coefficient for the wedge," *IEEE Trans. Antennas Propagat.*, vol. AP-32, pp. 175-177, Feb. 1984.
- [11] Y. Liu and I. R. Ciric, "Improved formulas for the diffraction by a wedge," *Radio Sci.*, vol. 28, no. 5, pp. 859-863, Sep./Oct. 1993.
- [12] S. W. Lee, Y. Rahmat-Samii, and R. C. Menendez, "GTD, ray field, and comments on two papers," *IEEE Trans. Antennas Propagat.*, vol. 26, pp. 352-354, Mar. 1978.
- [13] J. R. Mautz and R. F. Harrington, "Radiation and scattering from large polygonal cylinders transverse electric fields," *IEEE Trans. Antennas Propagat.*, vol. 24, pp. 469-477, July 1976.
- [14] M. Schneider and R. J. Luebbers, "A general uniform double wedge diffraction coefficient," *IEEE Trans. Antennas Propagat.*, vol. 39, 8-14, Jan. 1991.
- [15] R. G. Kouyoumjian, "The geometrical theory of diffraction and its applications," in *Numerical and Asymptotic Techniques in Electromagnetics*, R. Mittra, Ed. New York: Spring-Verlag, ch.6, pp. 167-251, 1975.
- [16] R. Tiberio and R. G. Kouyoumjian, "A uniform GTD solution for the diffraction by strips illustrated at grazing incidence," *Radio Sci.*, vol.14, no. 6, pp. 933-941, Nov.-Dec. 1979.
- [17] R. J. Luebbers, "A heuristic UTD slope diffraction coefficient for rough lossy wedges," *IEEE Trans. Antennas Propagat.*, vol. 37, pp. 206-211, Feb. 1989
- [18] J. Bach. Andersen, "UTD multiple-edge transition zone diffraction," *IEEE Trans. Antennas Propagat.*, vol. 45, no. 7, pp. 1093-1097, Jul. 1997.
- [19] J. H. Whitteker, "Fresnel-Kirchhoff theory applied to terrain diffraction problems," *Radio Sci.*, vol. 25, no. 5, pp. 837-851, Sept.-Oct. 1990.
- [20] J. H. Whitteker, "Diffraction over a flat-topped terrain obstacle," *Proc. IEE-H*, vol. 137, no. 2, pp. 113-116, Apr. 1990.
- [21] H. Mokhtari, "A Comprehensive double knife-edge diffraction computation method

- based on the complete Fresnel theory and a recursive series expansion method," *IEEE Trans. Veh. Technol.*, vol. 48, pp. 589-592, Mar. 1999.
- [22] J. H. Whittaker, "A series solution for diffraction over terrain modelled as multiple bridged knife edges," *Radio Sci.*, vol. 28, no. 4, pp. 487-500, Jul.-Aug. 1993.
- [23] Abramowitz, M. and I. A. Stegun, "Handbook of Mathematical Functions," *Appl. Math. Ser.*, vol. 55, National Bureau of Standards, Washington, D. C., 1964.
- [24] Y. Zhang, X. Zhao, Y. Xie, and G. Han, "The experimental study of frequency selective fading," *Journal of China Institute of Communications*, vol. 15, no. 6, pp. 1-8, Nov. 1994(in Chinese).
- [25] X. Zhao et al., "The progress on the study of frequency selective fading and depolarisation due to multipath propagation in China," *Journal of China Institute of Communications*, vol. 17, no. 3, pp. 8-14, May, 1996.
- [26] H. Jin, Z. Sha, and Y. Xie, "Distributions of the cross-polarization discrimination and the co-polarized attenuation due to multipath in clear air," *Radio Sci.*, vol. 22, no. 4, pp. 499-510, Jul.-Aug. 1987.
- [27] G. Yang et al., "The graphics of refractivity at low atmosphere in China," *Technical Report of China Research Institute of Radio wave Propagation*, Xinxiang, 1980.
- [28] Y. Zhang and Y. Xie, "Computer simulation of multipath fading for line-of-sight microwave links," *Chinese Journal of Radio Sci.*, vol. 4, no. 1, pp. 45-57, Mar. 1989.
- [29] C. Jiang et al., "Handbook of refraction and attenuation of radio wave propagation for radar," *Technical report of China Research Institute of Radio wave Propagation*, Xinxiang, 1997.
- [30] Y. Xie and C. Guo, "An experimental study on depolarization due to multipath propagation," *Acta Electron. Sin.*, vol. 15, no. 1, pp. 16-23, Jan. 1987 (in Chinese).
- [31] Rec. ITU-R P.530-6, *Propagation data and prediction methods required for the design of terrestrial line-of-sight systems*, Geneva, Switzerland, page 16, 1995.
- [32] ETSI HIPERLAN/1 standard,
<http://www.etsi.org/technicalactiv/Hiperlan/hiperlan1.htm>.
- [33] ETSI HIPERLAN/2 standard,
<http://www.etsi.org/technicalactiv/Hiperlan/hiperlan2.htm>.
- [34] R. van Nee and R. Prasad, *OFDM for Wireless Multimedia Communications*, Artech House, USA, 2000.
- [35] ETSI, Broadband Radio Access Networks (BRAN), HIPERLAN type 2 functional specification part 1- physical (PHY) layer, 1999.
- [36] W. C. Y. Lee, "Estimate of local average power of a mobile radio signal," *IEEE Trans. Veh. Technol.*, vol.34, no.1, pp. 22-27, Feb. 1985.
- [37] E. Green, "Radio link design for micro-cellular systems," *Br. Telecom Techol. J.*, vol. 8, no. 1, pp. 85-96, Jan. 1990.s
- [38] T. S. Rappaport, *Wireless Communications — Principles and Practice*, Prentice-Hall, Inc., New Jersey, 1996.
- [39] S.Y.Seidel and T. S. Rappaport, "914 MHz path loss prediction models for indoor wireless communications in multifloored buildings," *IEEE Trans. Antennas Propagat.*, vol. 40 no. 2, pp. 207-217, Feb. 1992.
- [40] L. Juan-Llacer, L . Ramos, and N. Cardona, "Application of some theoretical models for coverage prediction in macrocell urban environments," *IEEE Trans. Veh. Technol.*, vol. 48, no. 5, pp. 1463-1468, Sept. 1999.
- [41] J. F. Lafortune and M. Lecours, "Measurement and modelling of propagation losses in a building at 900 MHz," *IEEE Trans. Veh. Technol.*, vol. 39, no. 2, pp. 101-108, May 1990.
- [42] V. Erceg et al., "An empirically based path loss model for wireless channels in

- suburban environments,” *IEEE J. Select. Areas in Commun.*, vol. 17, no. 7, pp. 1205-1211, July 1999.
- [43] H. L. Bertoni, *Radio Propagation for Modern Wireless System*, Prentice Hall PTR, New Jersey, 2000.
- [44] J. M. Keenan and A. J. Motley, “Radio coverage in buildings,” *Br Telecom Technol J*, vol. 8, no. 1, pp. 19-24, Jan. 1990.
- [45] J. C-I Chuang, “The effects of time delay spread on portable radio communications channels with digital modulation,” *IEEE J. Select. Areas in Commun.*, vol. 5, no. 5, pp. 879-889, June 1987.
- [46] I. Crohn, G. Schultes, R. Gahleitner, and E. Bonek, “Irreducible error performance of a digital portable communication system in a controlled time-dispersion indoor channel,” *IEEE J. Select. Areas in Commun.*, vol. 11, no. 7, pp. 1024-1033, Sept. 1993.
- [47] A. F. Molisch, “A new method for the computation of the error probability of differentially detected modulation formats in mobile radio channels — the case of minimum shift keying,” *Wireless Personal Commun.*, vol. 9, no. 2, pp. 165-178, Feb. 1999.
- [48] A. F. Molisch, Editor, *Wideband Wireless Digital Communications*, Prentice Hall PTR, New Jersey, 2001.
- [49] U. Dersch and E. Zollinger, “Physical characteristics of urban micro-cellular propagation,” *IEEE Trans. Antennas Propagat.*, vol. 42, no. 11, pp. 1528-1539, Nov. 1994.
- [50] Y. Karasawa and H. Iwai, “Formulation of spatial correlation statistics in Nakagami-Rice fading environments,” *IEEE Trans. Antennas Propagat.*, vol. 48, no. 12, pp. 12-18, Jan. 2000.
- [51] H. Suzuki, “A statistical model for urban radio propagation,” *IEEE Trans. Commun.*, vol. 25, no. 7, pp. 673-680, July 1977.
- [52] S. Gao, *Study of multipath propagation in land mobile communications*, MSc. thesis, China Research Institute of Radio wave Propagation, Xinxiang, P. R. of China, pp. 5-21, 1995 (in Chinese).
- [53] S. Gao, S. Zhong, and C. Jiang, “Path number distribution for multipath propagation in land mobile communications and its simulation,” *Journal of China Institute of Communications*, vol. 19, no. 2, pp. 66-72, Feb. 1998 (in Chinese).
- [54] J. Tsao and B. D. Steinberg, “Reduction of side lobe and speckle artefacts in microwave imaging: the CLEAN technique,” *IEEE Trans. Antennas Propagat.*, vol. 36, no. 4, pp. 543-556, Apr. 1988.
- [55] H. Hashemi, “The indoor radio propagation channel,” *Proc. of IEEE*, vol. 81, no. 7, pp. 943-968, Jul. 1993.
- [56] K. K. Talukdar and W. D. Lawing, “Estimation of the parameters of the Rice distributions,” *J. Acoust. Soc. Amer.*, vol. 89, pp. 1193-1197, Mar. 1991.
- [57] A. Abdi, C. Tepedelenlioglu, M. Kaveh, and G. Giannakis, “On the estimation of the K parameter for Rice fading distribution,” *IEEE Commun. Letters*, vol. 5, no. 3, pp. 92-94, Mar. 2001.
- [58] L. J. Greenstein, D. G. Michelson, and V. Erceg, “Moment-method estimation of the Ricean K -factor,” *IEEE Commun. Letters*, vol. 3, no. 6, pp. 175-176, June 1999.
- [59] F. V. D. Wijk, A. Kegel, and R. Prasad, “Assessment of a pico-cellular system using propagation measurements at 1.9 GHz for indoor wireless communications,” *IEEE Trans. Vehicular Technol.*, vol. 44, no. 1, pp. 155-162, Feb. 1995.
- [60] W. Mohr, “Modeling of wideband mobile radio channel based on propagation measurements,” in *Proc. PIMRC’95*, Toronto, Canada, Sept. 27-29, 1995, pp. 397-401.
- [61] T. Ojanperä and R. Prasad, *Wideband CDMA for Third Generation Mobile Communications*, Artech House, USA, 1998.

- [62] R. H. Clarke, "A statistical theory of mobile-radio reception," *Bell Syst. Tech. J.*, pp. vol. 47, pp. 957-1000, July 1968.
- [63] T. Aulin, "A modified model for the fading signal at a mobile radio channel," *IEEE Trans. Veh. Technol.*, vol. 28, no. 3, pp. 182-203, Aug. 1979.
- [64] J. D. Parsons, *The mobile radio propagation channel*, Pentech Press, London, 1992.
- [65] T. Taga, "Analysis for mean effective gain of mobile antennas in land mobile radio environments," *IEEE Trans. Veh. Technol.*, vol. 39, no. 2, pp. 117-131, May 1990.
- [66] J. Bach. Andersen, "Angle-of-arrival statistics for low resolution antennas," *IEEE Trans. Antennas Propagat.*, vol. 50, no. 3, pp. 391-395, Mar. 2002.
- [67] K. Kalliola, *Experimental Analysis of Multidimensional Radio Channels*, Doctor Thesis, Helsinki University of Technology, Feb. 2002.
- [68] J. Fuhl, J. P. Rossi, and E. Bonek, "High-resolution 3-D direction-of-arrival determination for urban mobile radio," *IEEE Trans. Antennas Propagat.*, vol. 45, no. 4, pp. 672-682, Apr. 1997.
- [69] J. Medbo et. al., "Channel models for HIPERLAN/2 in different indoor scenarios," *COST 259 TD(98)070*, Bradford, UK, Apr. 23-24, 1998
- [70] P. A. Bello, "Characterization of randomly time-variant linear channels," *IEEE Trans. on Commun.*, vol. 11, pp. 360-393, Dec. 1963.
- [71] S. Kozono, "Received signal level characteristics in a wideband mobile radio channel," *IEEE Trans. Veh. Technol.*, vol. 43, no. 3, pp. 480-486, Aug. 1994.
- [72] J. Yan and S. Kozono, "A study of received signal level distribution in wideband transmissions in mobile communications," *IEEE Trans. Veh. Technol.*, vol. 48, no. 5, pp. 1718-1725, Sept. 1999.